Regional simulations of deep convection and biomass burning over South America: 2. Biomass burning aerosol effects on clouds and precipitation

Longtao Wu,[1] Hui Su,[1] and Jonathan H. Jiang[1]

Received 13 April 2011; revised 14 June 2011; accepted 16 June 2011; published 15 September 2011.

[1] A fully coupled meteorology-chemistry-aerosol mesoscale model (WRF-Chem) is used to simulate a multiday biomass burning event in the dry season of South America. The effects of biomass burning aerosols on clouds and precipitation are described at both 36 km and 4 km horizontal resolutions. The dominant effect of the aerosols is to reduce the diurnal amplitude of convection by decreasing clouds and precipitation in the afternoon but increasing them at night, with the afternoon decrease greater than the nighttime increase on the daily mean. On average, the decrease of surface precipitation is about 5% (3%) and the amplitude of diurnal cycle is reduced by about 11% (5%) in the 36 km (4 km) simulations. Such a modulation of clouds and precipitation is primarily contributed by the aerosol radiative effect, i.e., their ability to scatter and absorb solar radiation. The aerosol microphysical effect as cloud condensation nuclei tends to act oppositely to the aerosol radiative effect but with a smaller magnitude, especially in the simulations at 36 km horizontal resolution. The 4 km resolution runs exhibit similar behaviors to the 36 km simulations, with a slightly stronger role of the aerosol microphysical effect relative to the aerosol radiative effect. We find another important effect of biomass burning aerosols. When uplifted into the upper troposphere by deep convection, they can significantly warm the upper troposphere through their local radiative heating effect and result in significant moistening in the upper troposphere, potentially affecting the water vapor transport from the troposphere to the stratosphere.

Citation: Wu, L., H. Su, and J. H. Jiang (2011), Regional simulations of deep convection and biomass burning over South America: 2. Biomass burning aerosol effects on clouds and precipitation, *J. Geophys. Res.*, *116*, D17209, doi:10.1029/2011JD016106.

1. Introduction

[2] During the dry season of South America, biomass burning events inject a large amount of aerosols, mainly black carbon (BC) and organic carbon (OC), into the atmosphere. These aerosols can affect local weather and climate by two mechanisms: radiative and microphysical effects [*Kaufman and Koren*, 2006; *Rosenfeld et al.*, 2008]. The aerosol radiative effect is associated with the scattering and absorption of solar radiation. Aerosols can scatter the incoming solar radiation and cool both the surface and the atmosphere [*Charlson et al.*, 1992; *Kiehl and Briegleb*, 1993]. Absorbing aerosols, such as dust and BC, can also absorb solar radiation, which in turn heat the local atmosphere and possibly reduce cloud formation [*Hansen et al.*, 1997; *Koren et al.*, 2004]. The microphysical effect refers to aerosols serving as cloud condensation nuclei (CCN) and cloud ice nuclei (IN). By changing the size distribution of cloud droplets and ice particles, aerosol may affect internal cloud microphysics, cloud radiative properties and precipitation efficiency, thus affect the atmospheric hydrological cycle and energy balance [*Twomey*, 1977; *Jiang and Feingold*, 2006; *Rosenfeld et al.*, 2008]. The radiative and microphysical processes can also interact with each other and produce complicated aerosol effects on weather and climate system [*Koren et al.*, 2008; *Tao et al.*, 2007].

[3] Aerosols are distributed inhomogeneously in the horizontal and vertical, affected strongly by emission sources and atmospheric conditions. Accurate simulations of aerosol effects require fully coupled models for meteorology, chemistry and aerosols. However, many previous global and regional modeling studies were conducted with prescribed aerosols or simple modules without detailed gas-phase chemistry, aerosol microphysics, and aerosol-cloud interactions [e.g., *Tao et al.*, 2007; *Zhang et al.*, 2008; *Martins et al.*, 2009]. The development of the Weather Research and Forecasting model with Chemistry (WRF-Chem) provides us a useful tool to tackle the aerosol-cloud-precipitation interactions more realistically than before. *Gustafson et al.* [2007] showed that a fully coupled WRF-Chem can capture regional cloud variations better than uncoupled models.

[4] On short time scale, the diurnal cycle of solar radiation is a key driver for the local energy and water cycle variabilities.

[1]Aura Microwave Limb Sounder (MLS) Science Team, Jet Propulsion Laboratory, California Institute of Technology, Pasadena, California, USA.

0148-0227/11/2011JD016106

Table 1. Experiment Description

Experiment Identification	Experiment Description
PC36	Polluted Case at 36 km resolution.
CC36	Clean Case at 36 km resolution. The biomass burning emission is turned off.
PCNR36	Polluted Case at 36 km resolution without the radiation feedback from aerosol.
PCNR36_UT	Polluted Case at 36 km resolution without the radiation feedback from aerosol in the upper troposphere above model level 17 (~337 hPa).
PC4	Polluted Case at 4 km resolution.
CC4	Clean Case at 4 km resolution. The biomass burning emission is turned off.
PCNR4	Polluted Case at 4 km resolution. Without the radiation feedback from aerosol.

By modifying the incoming solar radiation, aerosols can modulate the diurnal changes of convection and cloud formation. In a WRF-Chem simulation over West Africa, *Zhao et al.* [2011] showed that dust reduced precipitation in late afternoon and increased precipitation at night and early morning by changing atmospheric stability. The decrease of daily mean precipitation was ~4% (0.17 mm/day). With an optimal geographical distribution of aerosol optical thickness (AOT) from the combination of the Moderate Resolution Imaging Spectro-radiometer (MODIS) retrievals and the Goddard Chemistry Aerosol Radiation and Transport (GOCART) model simulations, *Zhang et al.* [2008] investigated the radiative effect of biomass burning aerosols on the diurnal cycles of surface fluxes and planetary boundary layer (PBL) depth over South America. They found that aerosol radiative effects decreased clouds in the PBL and shifted the maximum changes of surface flux and the PBL depth to late morning. The strong absorption of solar radiation by aerosols was found about 2 to 3 km above the surface.

[5] In this study, the WRF-Chem model with fully coupled meteorology-aerosol-chemistry interactions is used to study biomass burning aerosol effects on clouds and precipitation in the dry season of South America. As described in the companion paper [*Wu et al.*, 2011], the South American region is chosen because previous observational data analysis [*Jiang et al.*, 2008] suggested a possible aerosol effect on the precipitation and cloud properties there. Our model simulations will address both aerosol radiative and microphysical effects by a series of sensitivity experiments. The model description and experiment design are documented in section 2. The impacts of aerosols on clouds and precipitation at 36 km resolution are discussed in section 3. Aerosol effects in the 4 km simulations are shown in section 4. section 5 is conclusion and discussion.

2. Model Description and Experiment Design

[6] We use the WRF-Chem [*Grell et al.*, 2005] Version 3.1.1 in this study. The details of model physical parameterization setups are documented by *Wu et al.* [2011]. Based on the fire locations from the geostationary NOAA weather satellite (GOES) fire data set WF_ABBA (www.nrlmry.navy.mil/flambe/index.html), biomass burning emissions are generated from the Brazilian Biomass Burning Emissions Model (3BEM), then injected into the atmosphere simulated by a plume rise model [*Freitas et al.*, 2005; *Grell et al.*, 2011]. Through a modal approach to representing the aerosol size distribution (Aiken, accumulation and coarse modes), aerosol evolution is simulated by the Regional Acid Deposition Model Version 2 (RADM2) [*Stockwell et al.*, 1990] photochemical mechanism coupled with the Modal Aerosol Dynamics Model for Europe (MADE/SORGAM) [*Ackermann et al.*, 1998; *Schell et al.*, 2001] aerosol mechanism. Aerosols are treated as "cloud borne" or "interstitial" based on whether they are activated to form clouds droplets [*Ghan and Easter*, 2006]. Aerosol activation follows the methodology used in the Megacities Impact on Regional and Global Environment (MIRAGE) general circulation model [*Abdul-Razzak and Ghan*, 2000, 2002; *Ghan et al.*, 1997, 2001a, 2001b; *Zhang et al.*, 2002]. Aerosol radiative effects are included through feedback from the aerosols to the Goddard shortwave radiation scheme [*Chou and Suarez*, 1994; *Fast et al.*, 2006; *Barnard et al.*, 2010]. By predicting the cloud droplet number concentration based on aerosol number concentration in the Lin et al. microphysics scheme [*Chen and Sun*, 2002; *Ghan et al.*, 1997], aerosol microphysical effects are included in the WRF-Chem [*Chapman et al.*, 2009]. The autoconversion of clouds to rain is also included based on the cloud droplet number [*Liu et al.*, 2005]. More details on the interactions between aerosols and clouds are provided by *Gustafson et al.* [2007], *Chapman et al.* [2009], *Barnard et al.* [2010] and *Grell et al.* [2011].

[7] The experiment design is listed in Table 1. The control simulation at 36 km horizontal resolution (Polluted Case, PC36) is initialized at 0000 UTC 15 September 2006 and run for 9 days. Considering the spin-up process in the first 24 h, our analysis starts from 0000 UTC 16 September 2006 for an 8-day period. The analysis is focused on the region where biomass burning occurred [*Wu et al.*, 2011, Figure 1a].

[8] The control simulation at 36 km resolution (PC36) has been evaluated with multisatellite observations and the results are detailed by *Wu et al.* [2011]. It has been shown that the model simulation at 36 km resolution reasonably reproduces the distribution and intensity of aerosols. The simulated precipitation agrees with the Tropical Rainfall Measuring Mission (TRMM) 3B42 data set, in both magnitude and temporal variation, although the precipitation locations are somewhat shifted. The spatial distribution of clouds is approximately reproduced although the magnitude of ice water content (IWC) and outgoing longwave radiation (OLR) at the top of the atmosphere (TOA) is weaker than observations. Given the reasonable performance of the model simulation, we are confident to use the model to examine aerosol effects on clouds and precipitation.

[9] Two sensitivity experiments are conducted at 36 km resolution. The biomass burning emission is turned off in the Clean Case (CC36) run (Table 1). Since the biomass burning emission is the primary source of aerosols (contributed to 76% of the AOT at 600 nm) in this study, the CC36 case is referred to as the clean environment. The total biomass burning aerosol effects can be evaluated by the difference between the PC36 and CC36 simulations. In the

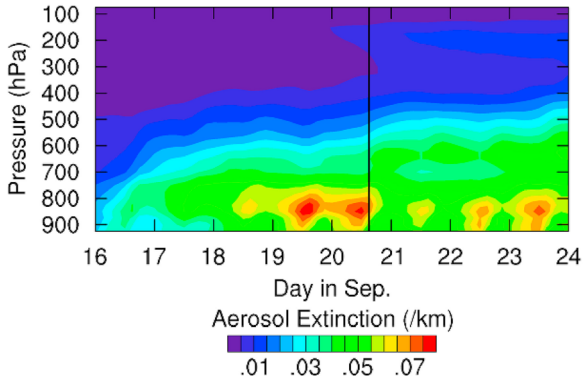

Figure 1. Domain-averaged difference of aerosol extinction coefficient (km^{-1}) between PC36 and CC36. Vertical black line is at 1500 UTC 20 September, 2006. Horizontal tick marks correspond to 0000 UTC, which is 20:00 P.M. one day before in local time (LST).

Polluted Case with No Radiation feedback (PCNR36) case (Table 1), the radiative feedback from aerosols to the radiation scheme is turned off so that the radiative effect of the aerosols (difference between the PC36 and PCNR36 simulations) can be accessed. The PCNR36 minus CC36 thus indicates mainly the microphysical effects of biomass burning aerosols although the radiative effects of non-biomass burning aerosols are present in CC36 but considerably small.

[10] At 36 km resolution, parameterized convection from the cumulus scheme contributes to the majority (89%) of surface precipitation while the remaining (11%) is contributed from the microphysical scheme [*Wu et al.*, 2011]. Aerosols effects as CCN are explicitly included in the Lin et al. microphysical scheme while they are not explicitly treated in the cumulus parameterization. Thus, we conduct similar sets of experiments at 4 km grid resolution, in which only the microphysical scheme is active. Due to computational constraint, the 4 km simulations are run with a smaller domain (inner domain of Figure 1a from *Wu et al.* [2011]) and a shorter time span (3 days). No cumulus scheme is used in all 4 km simulations. As shown by *Wu et al.* [2011], the control simulation at 4 km resolution (PC4) produced similar results to the 36 km control simulation (PC36). However, the 4-km simulated hydrometeor profile in the upper troposphere is closer to the Microwave Limb Sounder (MLS) observation while the 4-km surface precipitation has a high bias compared to the TRMM 3B42 rainfall product and the PC36 simulation.

3. Aerosol Effects at 36 km Resolution

3.1. Overall Effects in the 8-Day Simulation

[11] Figure 1 shows the domain-averaged difference in the aerosol extinction (AE) coefficient profiles between the PC36 and CC36 cases. The biomass burning event injects a large amount of aerosols into the atmosphere. The evolution of aerosols shows a clear signal of diurnal variation during the entire simulation period. The aerosols peak in the morning and are concentrated around 850 hPa. As time progresses, the aerosols are transported upward. From 1500 UTC 20 September (black vertical line in Figure 1) to the end of the simulation, a secondary maximum of aerosol layer is shown around 600 hPa. Between 300 hPa and 125 hPa, there is a distinct layer of aerosols, albeit with weak amplitude compared to the lower layers.

[12] The temperature difference between PC36 and CC36 runs shows the aerosols cool the surface and PBL while warm the local atmosphere where they reside (Figure 2a). A weak cooling is shown around 350 hPa, likely due to the changes in clouds as we discuss later. After 1500 UTC 20 September when the aerosols are transported to the upper troposphere, a relatively strong warming with a maximum of 0.39 K is produced in the upper troposphere around 200 hPa, collocated with the distinct aerosol layer. The ascending motion in the PBL (below 800 hPa) is suppressed in the afternoon (Figure 2b). In the middle and upper layers (above 800 hPa), the upward vertical velocity is enhanced in the afternoon but decreased at night. After 1500 UTC 20 September, the enhancement of ascent in the upper troposphere is further amplified, collocated with the distinct aerosol layer and intensive warming in the upper troposphere.

[13] The changes of the moisture profiles (Figure 3a) roughly follow the temperature changes. From 0000 UTC 16 September to 1500 UTC 20 September, increased moisture is shown in the middle layers below 500 hPa corresponding to the warming while reduced moisture is shown in higher altitudes between 500 and 200 hPa (Figure 3a). After September 20, significant drying and moistening occur around 300–500 hPa and above 300 hPa, respectively. The moistening reaches above 100 hPa with the amplitude up to 11% relative to the clean case.

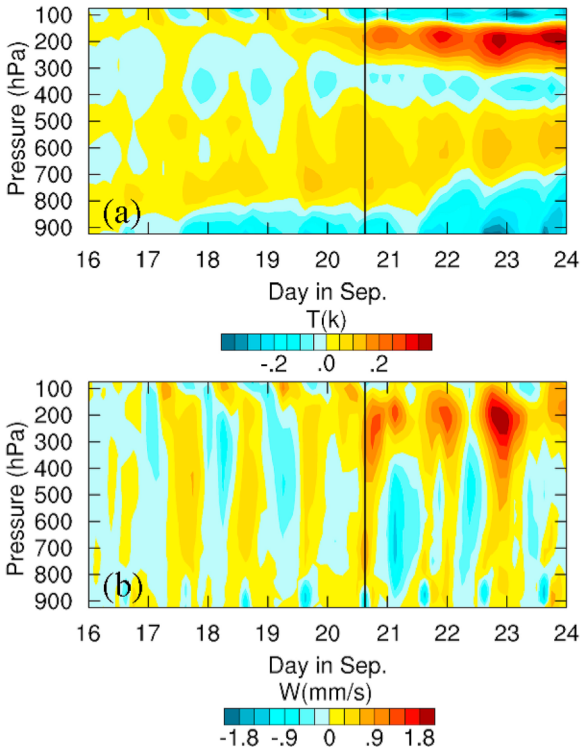

Figure 2. Domain-averaged difference between PC36 and CC36: (a) temperature (K); (b) vertical velocity (mm s^{-1}). Tick marks as Figure 1.

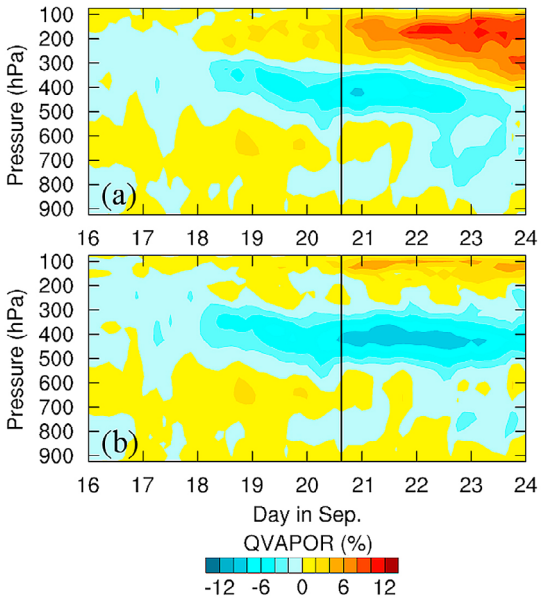

Figure 3. Domain-averaged relative difference of moisture (%): (a) between PC36 and CC36; (b) between PCNR36_UT and CC36. Tick marks as Figure 1.

[14] Increased aerosols in the PC36 run produce increased liquid clouds in the PBL below 825 hPa with the maximum increase occurring in the early morning (Figure 4). In the middle layers above 825 hPa, liquid clouds decrease in the afternoon but increase at night. There is also a tendency for ice clouds to decrease in the evening but to slightly elevate to a higher altitude in the early morning, especially after 1500 UTC 20 September.

[15] Affected by the biomass burning aerosols, surface precipitation is decreased by up to 0.15 mm (25%) compared to the clean case in the afternoon and increased by less than 0.04 mm (11%) in the midnight and early morning, suggesting a modulation of precipitation process by the aerosol effects (Figure 5). The increase of precipitation in the midnight and early morning is somewhat weakened after 1500 UTC 20 September. On the 8-day average, surface precipitation is reduced by about 5% and the amplitude (standard deviation) of precipitation diurnal cycle is reduced by about 11%. The aerosol impact on precipitation is consistent with findings of *Zhao et al.* [2011] except that they focused on the effects of African dust.

[16] For the radiative fluxes, aerosols reduce downward shortwave fluxes reaching the surface (SWDOWN) with the maximum reduction occurring at 1500 UTC 22 September (Figure 6a). OLR at TOA increases in the afternoon and slightly decreases in the early morning (Figure 6b), consistent with the changes of high-level ice clouds (see Figure 4). Averaged over the 8-day simulations, the SWDOWN decreases by 15.90 W m^{-2} while the OLR increases by 0.12 W m^{-2}.

[17] Overall, modest changes in clouds and precipitation as well as atmospheric temperature, water vapor and vertical motion are produced when biomass burning injects aerosols into the troposphere. Over the 8-day period, a clear diurnal variation of clouds and precipitation changes due to the increasing aerosols is present. Since the aerosol distributions and associated convective responses demonstrate distinctly different characteristics before and after 1500 UTC 20 September, we divide the simulation period into two phases, one from 0000 UTC 16 September to 1500 UTC 20 September, and the other from 1500 UTC 20 September to 0000 UTC 24 September. For each phase, we select one day to analyze in detail the aerosol effects on the diurnal cycle of the atmospheric system. In the first phase, we select the time period from 1500 UTC 19 September to 1500 UTC 20 September. In the second phase, we choose the time period from 1500 UTC 21 September to 1500 UTC 22 September for detailed analysis. *Fan et al.* [2009] showed that the impact of aerosols on deep convective clouds can be different under different vertical wind shear and other ambient synoptic conditions. Since the synoptic conditions before and after 1500 UTC 20 September are not significantly different, the impact of varying synoptic conditions on aerosol effects may be secondary.

3.2. Detailed Analysis for the First Phase

[18] As shown in the Figure 1, the AE shows maximum around 850 hPa in the morning of 19 September. Owing to the absorption of solar radiation by biomass burning aerosols, a maximum warming occurs around 750 hPa at 14:00 P.M. local time (Figure 7a). With the increased temperature, the middle-level clouds partly evaporate (Figure 7c), giving rise to increased moisture in the middle layer between 750 and 600 hPa (Figure 7e). Serving as CCN, the biomass burning aerosols led to the increase of cloud water mixing ratio and cloud droplet number concentration throughout the 24-h period in the first phase (Figure 7d and 7f). As the decrease of middle-level clouds caused by the aerosol radiative effect overcomes the increase of clouds due to the aerosol microphysical effect, the net decrease of middle-level clouds is produced in the afternoon (Figure 7b). Due to the aerosol absorption of solar radiation, the warming of middle layers causes increased vertical ascending motion in the afternoon, with maxima around 400 hPa (Figure 7a). Collocated with the enhanced vertical ascent, moisture is transported upward, yielding a moistening from 300 hPa to 100 hPa and a drying between 600 and 300 hPa (Figure 7e).

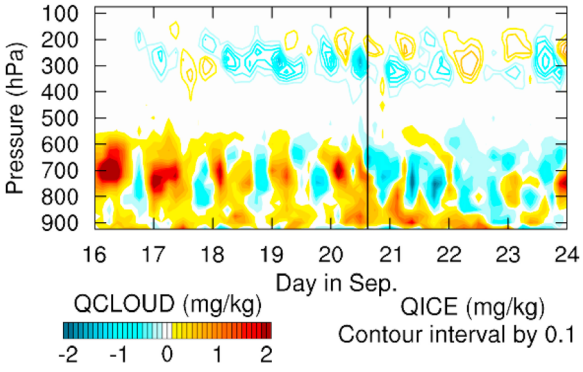

Figure 4. Domain-averaged difference of clouds (mg kg^{-1}) between PC36 and CC36. Color shadings are liquid clouds. Color contours are ice clouds with 0.1 mg kg^{-1} interval; zero line is not shown. Yellow indicates positive values and cyan indicates negative values. Tick marks as Figure 1.

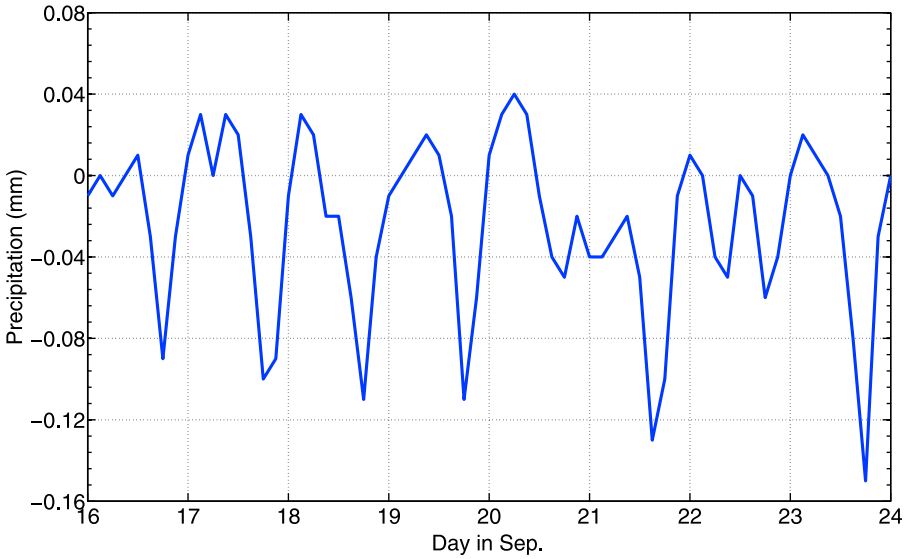

Figure 5. Domain-averaged difference of 3-h surface precipitation (mm) between PC36 and CC36. Tick marks as Figure 1.

[19] Aerosols also scatter the incoming solar radiation. Both scattering and absorption decrease the solar radiation reaching the surface, resulting in cooling at the surface and in the PBL in the afternoon (Figure 7a). Such cooling suppresses the vertical ascent in the PBL (Figure 7a) while it slightly increases the boundary layer clouds (Figure 7c) due to the increase of relative humidity.

[20] The decrease of middle-level clouds in the afternoon affects the upper-level clouds and precipitation processes in the afternoon and evening (Figure 7). In the evening around 20:00 P.M., a decrease of ice clouds occurs (Figure 7b) partly because less liquid clouds are available to be uplifted above freezing level to form ice clouds. The decrease of moisture between 300 hPa and 600 hPa (Figure 7e) may also contribute to the decrease of ice clouds. The air temperature around 350 hPa decreases (Figure 7a) due to reduced latent heat release from ice formation.

[21] When the warming of the atmosphere due to the absorption of solar radiation is not active at night, there is a slightly suppression of upward motion in the middle layers with the peak suppression around 23:00 P.M. (Figure 7a) and an increase of middle-level clouds (Figure 7b), due to the combined aerosol radiative and microphysical effects (Figures 7c and 7d). The aerosol radiative effect increases moisture availability at night (Figure 7e) owing to the evaporation of clouds in the afternoon (Figure 7c), while the microphysical effect facilitates cloud formation by providing CCN (Figure 7d). The increase of liquid clouds in the

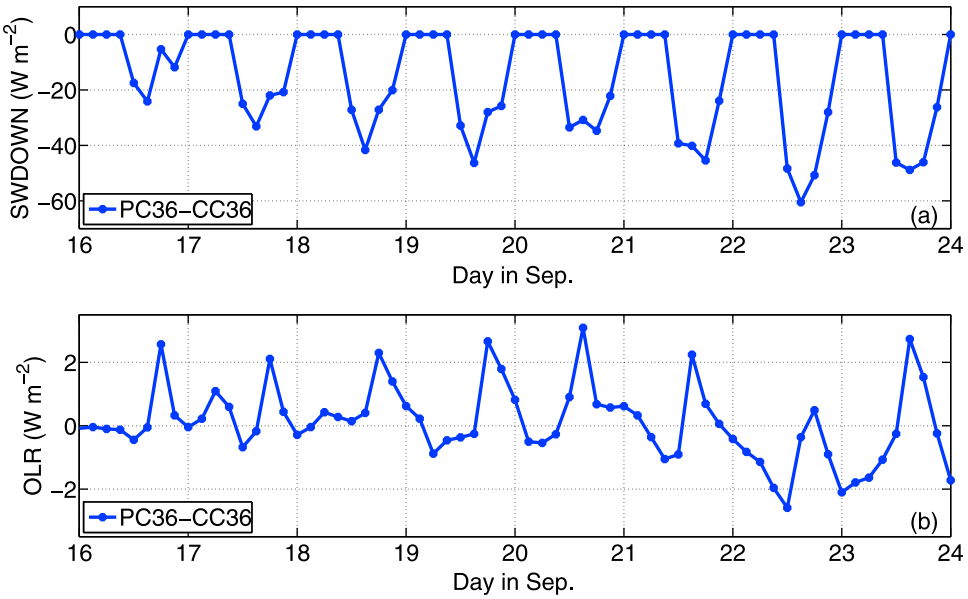

Figure 6. Domain-averaged difference of radiation fluxes (W m^{-2}). (a) SWDOWN; (b) OLR at TOA. Tick marks as Figure 1.

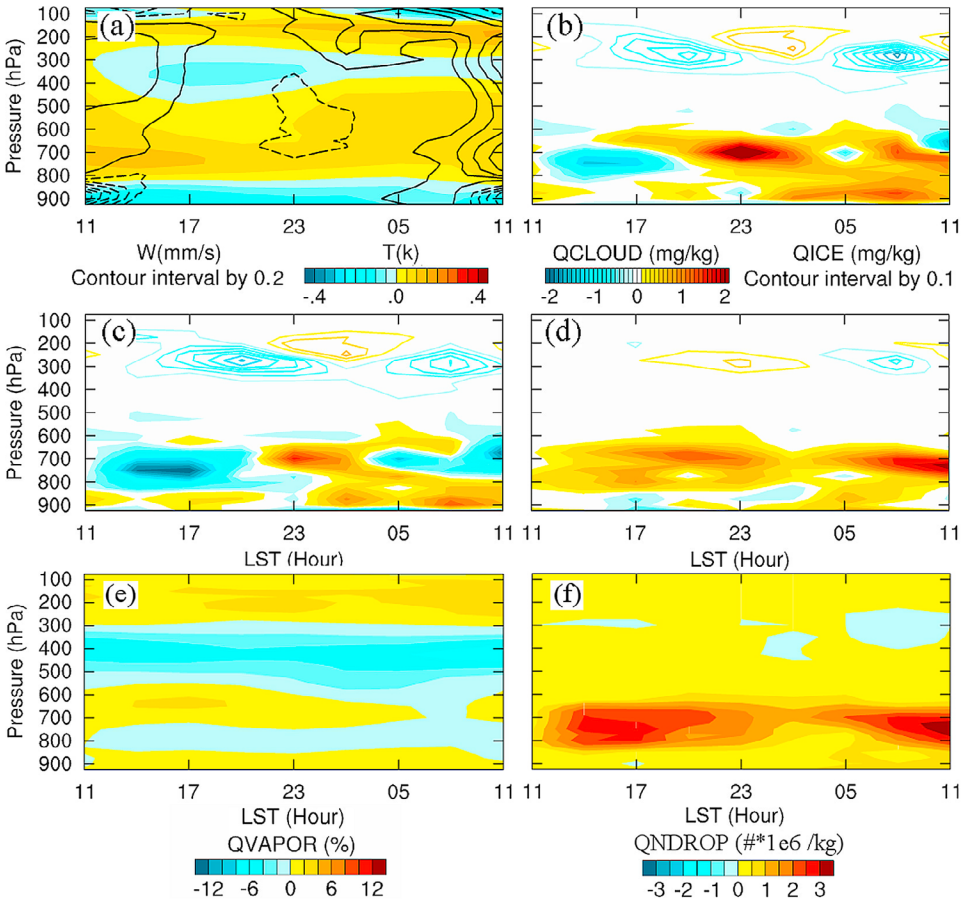

Figure 7. Aerosol effects in the first phase. (a) Aerosol total effects on temperature (color; K) and vertical velocity (contour with interval by 0.2 mm s^{-1}; zero line is not shown): difference between PC36 and CC36; (b) aerosol total effects on clouds (mg kg^{-1}): differences of liquid (color) and ice (contour with interval by 0.1 mg kg^{-1}; zero line is not shown) clouds between PC36 and CC36; (c) aerosol radiative effects on clouds (mg kg^{-1}): differences of liquid (color) and ice (contour) clouds between PC36 and PCNR36; (d) aerosol microphysical effects on clouds (mg kg^{-1}): differences of liquid (color) and ice (contour) clouds between PCNR36 and CC36. (e) Aerosol total effects on moisture (%) in the first phase: relative difference between PC36 and CC36. (f) Aerosol microphysical effect on cloud droplet number concentration (# × 10^6 kg^{-1}): difference between PCNR36 and CC36. Horizontal axis is local time on Sep. 20, 2006.

middle layers leads to more ice clouds in the upper levels. The increase of moisture in the upper troposphere may also help ice cloud formation. In addition, increasing aerosols as CCN decrease the cloud droplet size so that smaller cloud droplets can be transported to higher altitudes. Hence, an increase of ice clouds is seen at night, peaking around 2:00 A.M. (Figure 7b). As shown in Figure 5, there is a small increase of surface precipitation in the early morning. Enhanced precipitation reduces cloud water in the early morning from 5:00 A.M. to 8:00 A.M. (Figure 7b). The middle atmosphere experiences warming because of the latent heat release of condensation (Figure 7a).

3.3. Detailed Analysis for the Second Phase

[22] In the second phase, more aerosols are transported upward to the middle and upper troposphere while a lesser amount of aerosol stays in the lower troposphere (Figure 1). A distinct layer of aerosols is shown between 125 hPa and 300 hPa. The second phase (Figure 8) displays some similar aerosol effects to the first phase (Figure 7), including cooling of the PBL, warming of the middle atmosphere and suppression of clouds in the afternoon, etc. However, it also shows some different features from the first phase because of the different aerosol concentration and elevation.

[23] Comparing to the first phase, the middle-layer aerosol warming effect in the second phase (Figure 8a) extends to longer time with the maximum at a higher altitude. In the second phase, the suppression of upward motion is delayed to 5:00 P.M. and only enhanced in the evening and at night (Figure 8a). The extended warming in the middle atmosphere inhibits cloud formation (Figure 8c) throughout the 24-h period, while such cloud inhibition ceases around 23:00 P.M. in the first phase (Figure 7c).

[24] Although the concentration of aerosols is relatively small in the upper troposphere between 125 hPa and 300 hPa, they can exert a strong heating to the atmosphere because of the low air density there (Figure 8). Amplified warming and ascending (Figure 8a) are shown in the upper

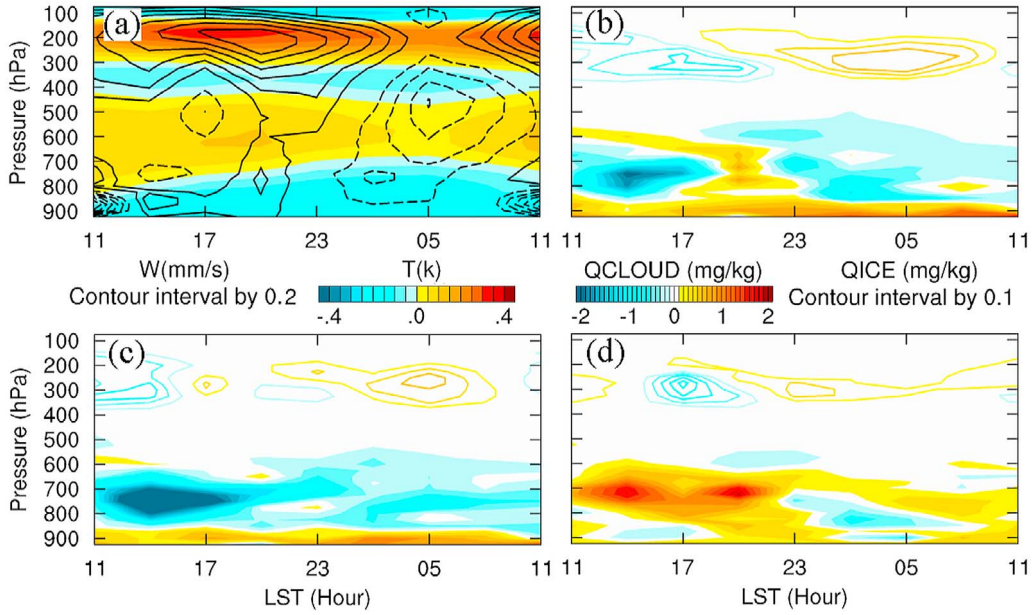

Figure 8. Aerosol effects in the second phase. (a) Aerosol total effects on temperature (color; K) and vertical velocity (contour with interval by 0.2 mm s^{-1}; zero line is not shown): difference between PC36 and CC36; (b) aerosol total effects on clouds (mg kg^{-1}): differences of liquid (color) and ice (contour with interval by 0.1 mg kg^{-1}; zero line is not shown) clouds between PC36 and CC36; (c) aerosol radiative effects on clouds (mg kg^{-1}): differences of liquid (color) and ice (contour) clouds between PC36 and PCNR36; (d) aerosol microphysical effects on clouds (mg kg^{-1}): differences of liquid (color) and ice (contour) clouds between PCNR36 and CC36. Horizontal axis is local time on Sep. 22, 2006.

troposphere collocated with the enhanced aerosol concentration. The increased vertical motion transports more moisture upward into the upper troposphere (Figure 3a), leading to a moistening up to 11% between 300 and 125 hPa accompanied by a drying below 300 hPa (Figure 3a). Consequently, an increase of cloud ice above 300 hPa is shown at night till early morning (Figure 8c).

[25] In order to distinguish the radiative effect of the upper tropospheric aerosols from the other aerosol effects, we conduct an experiment in which only the aerosol radiative effect in the upper troposphere is turned off (the PCNR36_UT case in Table 1) and the rest is the same as the control experiment. Comparing Figure 3b with Figure 3a, we can see that the amplified moistening in the upper troposphere is mainly due to the aerosol radiative effect in the upper troposphere but other aerosol effects also play a role. Current model microphysical scheme does not treat aerosols as IN; thus the aerosol microphysical effect in the upper troposphere may be underestimated.

4. Aerosol Effects at the 4 km Resolution

[26] In order to minimize the uncertainties arising from the cumulus scheme, which does not explicitly include aerosol effects, we conduct similar sets of experiments at 4 km resolution for a shorter time period. In the 4 km simulations, all clouds are explicitly produced from the microphysical scheme. The 4 km simulations produce similar aerosol distributions to the 36 km simulations (Figure 9a and 9c). However, the magnitude of biomass burning aerosols is smaller in the 4 km simulations, which partly results from heavier precipitation in the 4 km simulations (shown by *Wu et al.* [2011]). The aerosol effects on clouds in the 4 km simulations are consistent with the results shown in the 36 km simulations (Figure 9b and 9d). The differences between the PC4 and CC4 runs show that biomass burning aerosols decrease liquid and ice clouds in the afternoon and increase them at night and/or in the early morning. The decrease of middle-level clouds in the afternoon is due to the radiative effects of the aerosols while they provide more moisture to form clouds at night (Figure 9e). During the entire simulation, the aerosol microphysical effect (Figure 9f) increases middle-level clouds by providing more CCN, with two maxima, one in early morning and one at night. The overall evolution of aerosol radiative and microphysical effects on clouds in the 4 km simulations (Figure 9) are qualitatively similar to those in the 36 km simulations (Figure 7). Partially due to the weaker aerosol concentrations, the magnitude of cloud changes in the 4 km simulations is smaller than that in the 36 km simulations. The aerosol effects on temperature and vertical velocity in the 4 km simulations (Figure 9g and 9h) also show similar patterns to those in the 36 km simulations (Figure 2), except with weaker amplitude.

[27] In the 36 km simulations, the biomass burning aerosols suppress surface precipitation in the afternoon and slightly enhance it at night (Figure 5 and Figure 10). Both the suppression and enhancement are mainly contributed by the aerosol radiative effect (Figure 10). The aerosol microphysical effect generally opposes to the aerosol radiative effect in the 36 km simulations with a relatively small magnitude. The aerosol effects on surface precipitation in the 4 km simulations (dashed lines in Figure 10) are approximately similar to the 36 km simulations (solid lines

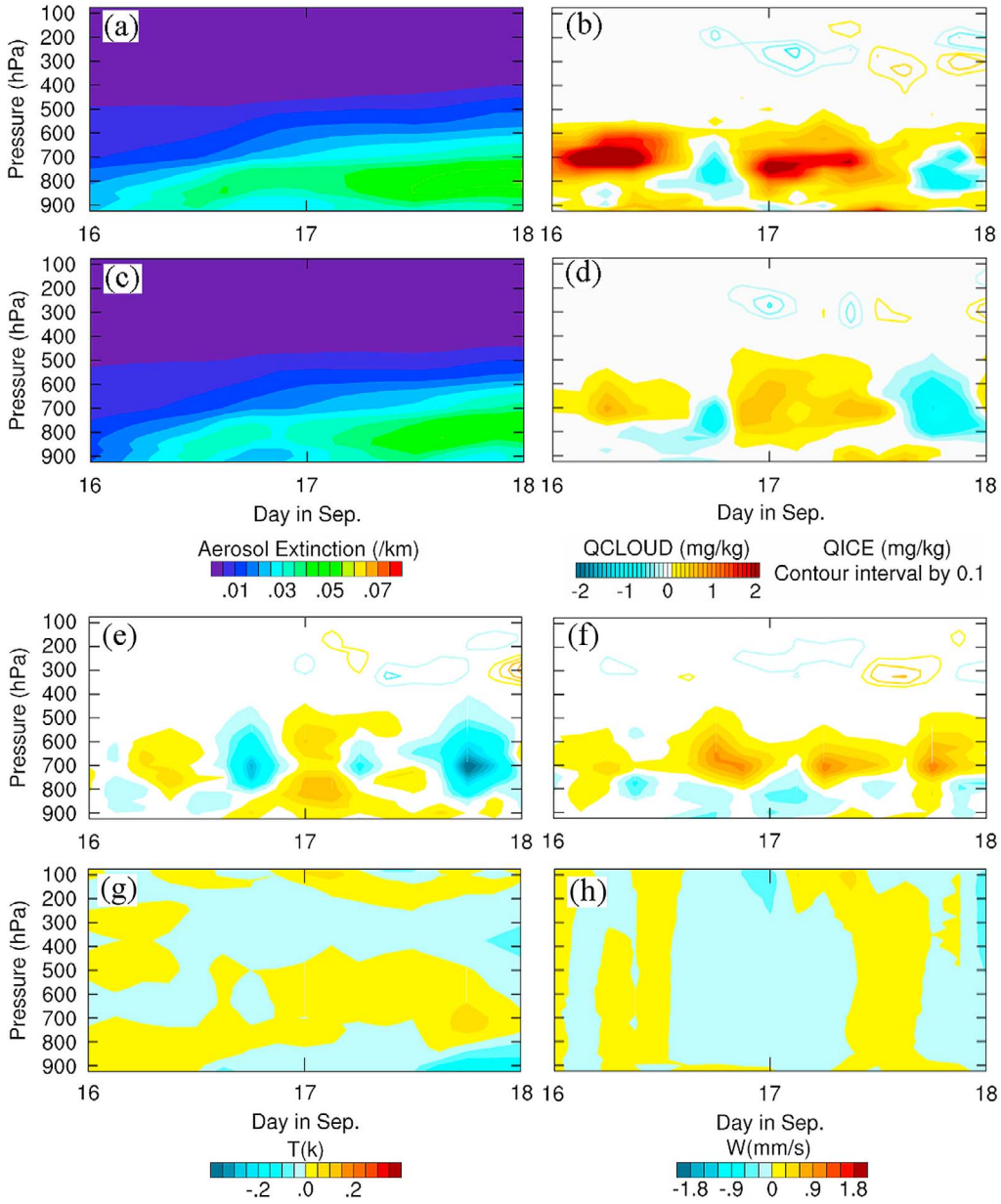

Figure 9. (a) Difference of aerosol extinction (km^{-1}) between PC36 and CC36; (b) difference of liquid (color) and ice (contour with interval by 0.1 mg kg^{-1}; zero line is not shown) clouds (mg kg^{-1}) between PC36 and CC36; (c) difference of aerosol extinction (km^{-1}) between PC4 and CC4; (d) difference of liquid (color) and ice (contour) clouds (mg kg^{-1}) between PC4 and CC4. (e) Difference of liquid (color) and ice (contour) clouds (mg kg^{-1}) between PC4 and PCNR4; (f) difference of liquid (color) and ice (contour) clouds (mg kg^{-1}) between PCNR4 and CC4; (g) difference of temperature (K) between PC4 and CC4; (h) difference of vertical velocity (mm s^{-1}) between PC4 and CC4. Horizontal tick marks correspond to 0000 UTC, which is 20:00 P.M. one day before in LST.

in Figure 10), with suppression of precipitation in the afternoon and enhancement at night, but to a lesser extent. In the 4 km simulations, the enhancement of precipitation at night does not last long into early morning because the timing of the peak aerosol radiative and microphysical effects is shifted earlier compared to the 36 km simulations. The relative magnitude of microphysical effect in the 4 km appears greater than in the 36 km. On the 2-day average, surface precipitation is reduced by about 3% and the amplitude of precipitation diurnal cycle is reduced by about 5%. Overall, the two different resolution runs produce qualitatively consistent results.

5. Conclusion and Discussion

[28] In this study, the biomass burning aerosol effects on clouds and precipitation in the dry season of South America are investigated using the fully coupled WRF-Chem model

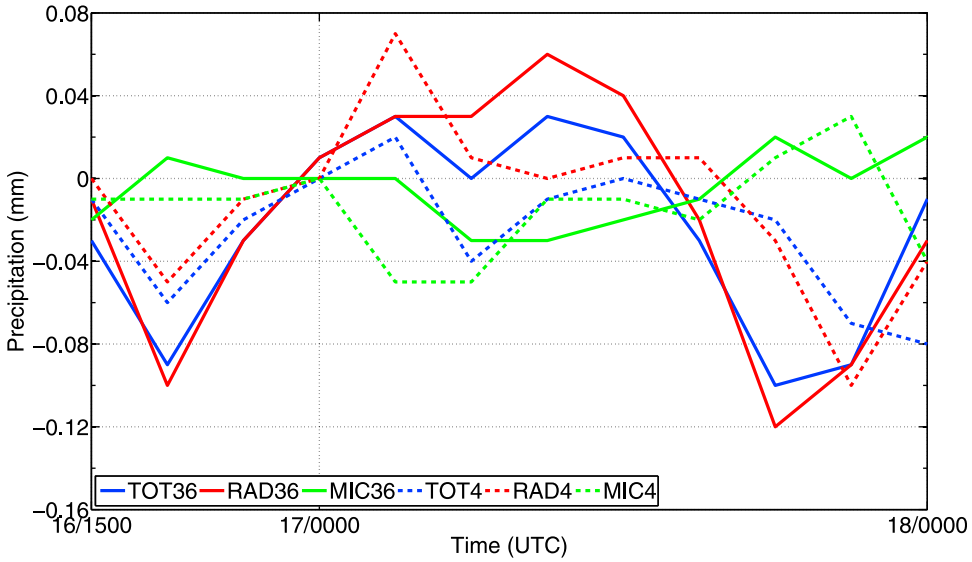

Figure 10. Aerosol affected 3-h accumulated surface precipitation (mm). Solid lines are from the 36 km simulations while dashed lines are from the 4 km simulations. Total effect (PC-CC): blue; Radiative effect (PC-PCNR): red; Microphysical effect (PCNR-CC): green. Time is from 1500 UTC 16 September to 0000 UTC 18 September, 2006.

at two grid resolutions, 36 km and 4 km. It is shown that the aerosol effects suppress surface precipitation in the daytime and enhance it at night, resulting in a reduced amplitude for the diurnal cycle of precipitation by about 11% (5%) in the 36 km (4 km) simulations. On the average of the 8-day (2-day) simulations, biomass burning aerosols suppress precipitation by 5% (3%) at 36 km (4 km) resolution. Clouds decrease in the afternoon and increase at night and in the early morning. The SWDOWN decreases by 15.90 W m^{-2} while the OLR at TOA increases by 0.12 W m^{-2} averaged for the 8-day simulations, corresponding to an overall decrease of high level clouds.

[29] BC and OC are primary aerosol types for biomass burning aerosols. The aerosol effects that manifest in our simulations predominantly result from the absorption of solar radiation by the absorptive aerosol BC. Both BC and OC scatter solar radiation but the cooling effect is largely confined within the PBL near the surface. The changes of the local water cycle (clouds, precipitation and water vapor) bear a clear diurnal variability, directly pointing to the predominance of the aerosol radiative effect as the aerosol microphysical effect does not necessarily imply a strong diurnal oscillation. For multiday averages, the aerosol microphysical effect may be more important as the diurnal changes due to the aerosol radiative effect largely cancel out. Our results are consistent with the earlier observational analysis by *Jiang et al.* [2008], i.e., biomass burning aerosols over South America tend to reduce precipitation on long-term averages.

[30] The modulation of the diurnal cycle of clouds and precipitation is a consequence of coupled aerosol-meteorology interactions. For example, the warming of middle layers due to aerosol absorption dissipates clouds in the afternoon but increases moisture. At night, when the aerosol warming ceases to act, the enhanced moisture promotes cloud growth and precipitation. The temperature and vertical velocity changes are initiated by aerosol radiative effects, but are further modified by consequent convection, such as the latent heat release due to condensation. We find hints of "cloud invigoration" as hypothesized by *Rosenfeld et al.* [2008] in that ice clouds are increased and elevated higher (at night) when aerosols act as CCN, compared to the clean environment (Figure 7d). However, such "cloud invigoration" is not as evident in the 4 km simulations (Figure 9d) as in the 36 km simulations. Due to the imperfect simulations of ice clouds in the model [*Wu et al.*, 2011], caution needs to be exercised when interpreting the results.

[31] When the biomass burning aerosols are transported into the upper troposphere, significant upper tropospheric warming and moistening are produced primarily owing to the absorption of solar radiation by the aerosols. For the same amount of aerosol concentrations, the aerosol heating effect is much stronger in the upper troposphere than in the lower levels. In our simulations after 1500 UTC 20 September, the AE between 125 and 300 hPa is only about 23% of that for the layer between 500 and 675 hPa. However, the aerosol induced atmospheric warming in the upper troposphere is about 2 times of that in the lower layers. This suggests a potentially important pathway for aerosols to impact the water transport from the troposphere to the stratosphere. *Su et al.* [2011] analyzed satellite observations and showed aerosols over South East Asia may cause increased temperature and water vapor in the tropical tropopause layer (TTL). Our model simulations indicate that the radiative heating of absorbing aerosols in the upper troposphere may be an important mechanism for the relations between observed aerosol and TTL temperature and water vapor. Observations, such as the Cloud-Aerosol Lidar and Infrared Pathfinder Satellite Observations (CALIPSO) data, show that aerosols can be transported to the upper troposphere in a deep

convective system [*Wu et al.*, 2011]. Further investigation will be conducted to quantify the aerosol effects on the water vapor transport across the tropopause.

[32] The 36 km simulations and 4 km simulations show similar aerosol effects, including the relative roles of aerosol radiative effect and microphysical effect, despite of the use of cumulus parameterization scheme in the 36 km simulation. This suggests that using WRF-Chem at a meso-scale grid resolution (a few tens of kilometers) is acceptable for regional studies of aerosol effects. However, the magnitude of aerosol concentration in the 4 km simulation is somewhat weaker than that in the 36 km simulations, which may affect the quantitative comparison between the 36 km runs and the 4 km runs.

[33] However, some caveats should be noted in this study. First, this study is only an 8-day case study. Longer period simulations should be conducted in order to obtain a climatic effect of biomass burning aerosols. Second, the cumulus parameterization is used in the 36 km simulations. As aerosol effects are not explicitly included in the cumulus schemes in the current WRF-Chem, improvements to the cumulus schemes are needed to better quantify the role of aerosols. Moreover, aerosols are not treated as IN in the current microphysical schemes in the WRF-Chem. Efforts are ongoing to update the model microphysical schemes. Continued investigation of aerosol effects, especially their impacts on climate, will be carried out.

[34] **Acknowledgments.** The authors thank Chun Zhao, Steven Peckham, Mary Barth, Xiaohong Liu, Xiaoming Hu and the WRF support staff for their assistance with running the WRF-Chem simulations. The authors also thank Jerome Fast, Georg Grell and Minghuai Wang for valuable suggestions. The comments from three anonymous reviewers are appreciated. This study was supported by NASA IDS and AST programs, as well as the Aura MLS project. The work is conducted at the Jet Propulsion Laboratory, California Institute of Technology, under contract with NASA.

References

Ackermann, I. J., H. Hass, M. Memmesheimer, A. Ebel, F. S. Binkowski, and U. Shankar (1998), Modal aerosol dynamics model for Europe: Development and first applications, *Atmos. Environ.*, *32*(17), 2981–2999, doi:10.1016/S1352-2310(98)00006-5.

Abdul-Razzak, H., and S. J. Ghan (2000), A parameterization of aerosol activation: 2. Multiple aerosol types, *J. Geophys. Res.*, *105*(D5), 6837–6844, doi:10.1029/1999JD901161.

Abdul-Razzak, H., and S. J. Ghan (2002), A parameterization of aerosol activation: 3. Sectional representation, *J. Geophys. Res.*, *107*(D3), 4026, doi:10.1029/2001JD000483.

Barnard, J. C., J. D. Fast, G. Paredes-Miranda, W. P. Arnott, and A. Laskin (2010), Technical Note: Evaluation of the WRF-Chem "Aerosol Chemical to Aerosol Optical Properties" Module using data from the MILAGRO campaign, *Atmos. Chem. Phys.*, *10*, 7325–7340, doi:10.5194/acp-10-7325-2010.

Chapman, E. G., W. I. Gustafson Jr., R. C. Easter, J. C. Barnard, S. J. Ghan, M. S. Pekour, and J. D. Fast (2009), Coupling aerosol-cloud-radiative processes in the WRF-Chem model: Investigating the radiative impact of elevated point sources, *Atmos. Chem. Phys.*, *9*, 945–964, doi:10.5194/acp-9-945-2009.

Charlson, R. J., S. E. Schwartz, J. H. Hales, R. D. Cess, J. A. Coakley Jr., J. E. Hansen, and D. J. Hofmann (1992), Climate forcing by anthropogenic aerosols, *Science*, *255*, 423–430, doi:10.1126/science.255.5043.423.

Chen, S.-H., and W.-Y. Sun (2002), A one-dimensional time dependent cloud model, *J. Meteorol. Soc. Jpn.*, *80*, 99–118, doi:10.2151/jmsj.80.99.

Chou, M.-D., and M. J. Suarez (1994), An efficient thermal infrared radiation parameterization for use in general circulation models, *NASA Tech. Memo., TM-104606*, vol. 3, 85 pp., NASA Goddard Space Flight Cent., Greenbelt, Md.

Fan, J., T. Yuan, J. M. Comstock, S. Ghan, A. Khain, L. R. Leung, Z. Li, V. J. Martins, and M. Ovchinnikov (2009), Dominant role by vertical wind shear in regulating aerosol effects on deep convective clouds, *J. Geophys. Res.*, *114*, D22206, doi:10.1029/2009JD012352.

Fast, J. D., W. I. Gustafson Jr., R. C. Easter, R. A. Zaveri, J. C. Barnard, E. G. Chapman, G. A. Grell, and S. E. Peckham (2006), Evolution of ozone, particulates, and aerosol direct radiative forcing in the vicinity of Houston using a fully coupled meteorology-chemistry-aerosol model, *J. Geophys. Res.*, *111*, D21305, doi:10.1029/2005JD006721.

Freitas, S. R., K. M. Longo, M. Silva Dias, P. Silva Dias, R. Chatfield, E. Prins, P. Artaxo, G. Grell, and F. Recuero (2005), Monitoring the transport of biomass burning emissions in South America, *Environ. Fluid Mech.*, *5*(1–2), 135–167, doi:10.1007/s10652-005-0243-7.

Ghan, S. J., and R. C. Easter (2006), Impact of cloud-borne aerosol representation on aerosol direct and indirect effects, *Atmos. Chem. Phys.*, *6*, 4163–4174, doi:10.5194/acp-6-4163-2006.

Ghan, S. J., L. R. Leung, R. C. Easter, and H. Abdul-Razzak (1997), Prediction of cloud droplet number in a general circulation model, *J. Geophys. Res.*, *102*(D18), 21,777–21,794, doi:10.1029/97JD01810.

Ghan, S. J., R. C. Easter, E. G. Chapman, H. Abdul-Razzak, Y. Zhang, L. R. Leung, N. S. Laulainen, R. D. Saylor, and R. A. Zaveri (2001a), A physically based estimate of radiative forcing by anthropogenic sulfate aerosol, *J. Geophys. Res.*, *106*(D6), 5279–5293, doi:10.1029/2000JD900503.

Ghan, S. J., R. C. Easter, J. Hudson, and F.-M. Breon (2001b), Evaluation of Aerosol Indirect Radiative Forcing in MIRAGE, *J. Geophys. Res.*, *106*(D6), 5317–5334, doi:10.1029/2000JD900501.

Grell, G. A., S. E. Peckham, R. Schmitz, S. A. McKeen, G. Frost, W. C. Skamarock, and B. Eder (2005), Fully coupled "online" chemistry within the WRF model, *Atmos. Environ.*, *39*, 6957–6975, doi:10.1016/j.atmosenv.2005.04.027.

Grell, G., S. R. Freitas, M. Stuefer, and J. Fast (2011), Inclusion of biomass burning in WRF-Chem: Impact of wildfires on weather forecasts, *Atmos. Chem. Phys.*, *11*, 5289–5303, doi:10.5194/acp-11-5289-2011.

Gustafson, W. I., Jr., E. G. Chapman, S. J. Ghan, R. C. Easter, and J. D. Fast (2007), Impact on modeled cloud characteristics due to simplified treatment of uniform cloud condensation nuclei during NEAQS 2004, *Geophys. Res. Lett.*, *34*, L19809, doi:10.1029/2007GL030021.

Hansen, J., M. Sato, and R. Ruedy (1997), Radiative forcing and climate response, *J. Geophys. Res.*, *102*(D6), 6831–6864, doi:10.1029/96JD03436.

Jiang, H., and G. Feingold (2006), Effect of aerosol on warm convective clouds: Aerosol-cloud-surface flux feedbacks in a new coupled large eddy model, *J. Geophys. Res.*, *111*, D01202, doi:10.1029/2005JD006138.

Jiang, J. H., H. Su, M. Schoeberl, S. T. Massie, P. Colarco, S. Platnick, and N. Livesey (2008), Clean and polluted clouds: Relationships among pollution, ice cloud and precipitation in South America, *Geophys. Res. Lett.*, *35*, L14804, doi:10.1029/2008GL034631.

Kaufman, Y. J., and I. Koren (2006), Smoke and pollution aerosol effect on cloud cover, *Science*, *313*, 655–658, doi:10.1126/science.1126232.

Kiehl, J., and B. Briegleb (1993), The relative roles of sulfate aerosols and greenhouse gases in climate forcing, *Science*, *260*, 311–314, doi:10.1126/science.260.5106.311.

Koren, I., Y. J. Kaufman, L. A. Remer, and J. V. Martins (2004), Measurement of the effect of Amazon smoke on inhibition of cloud formation, *Science*, *303*, 1342–1345, doi:10.1126/science.1089424.

Koren, I., J. V. Martins, L. A. Remer, and H. Afargan (2008), Smoke invigoration versus inhibition of clouds over the Amazon, *Science*, *321*(5891), 946–949, doi:10.1126/science.1159185.

Liu, Y., P. H. Daum, and R. L. McGraw (2005), Size truncation effect, threshold behavior, and a new type of autoconversion parameterization, *Geophys. Res. Lett.*, *32*, L11811, doi:10.1029/2005GL022636.

Martins, J. A., M. A. F. Silva Dias, and F. L. T. Gonçalves (2009), Impact of biomass burning aerosols on precipitation in the Amazon: A modeling case study, *J. Geophys. Res.*, *114*, D02207, doi:10.1029/2007JD009587.

Rosenfeld, D., U. Lohmann, G. B. Raga, C. D. O'Dowd, M. Kulmala, S. Fuzzi, A. Reissell, and M. O. Andreae (2008), Flood or drought: How do aerosols affect precipitation?, *Science*, *321*, 1309–1313, doi:10.1126/science.1160606.

Schell, B., I. J. Ackermann, H. Hass, F. S. Binkowski, and A. Ebel (2001), Modeling the formation of secondary organic aerosol within a comprehensive air quality model system, *J. Geophys. Res.*, *106*(D22), 28,275–28,293, doi:10.1029/2001JD000384.

Stockwell, W. R., P. Middleton, J. S. Chang, and X. Tang (1990), The second generation regional acid deposition model chemical mechanism for regional air quality modeling, *J. Geophys. Res.*, *95*(D10), 16,343–16,367, doi:10.1029/JD095iD10p16343.

Su, H., J. H. Jiang, X. Liu, J. E. Penner, W. G. Read, S. T. Massie, M. R. Schoeberl, P. Colarco, N. J. Livesey, and M. L. Santee (2011), Observed increase of TTL temperature and water vapor in polluted clouds over Asia, *J. Clim.*, *24*, 2728–2736, doi:10.1175/2010JCLI3749.1.

Tao, W.-K., X. Li, A. Khain, T. Matsui, S. Lang, and J. Simpson (2007), Role of atmospheric aerosol concentration on deep convective precipitation: Cloud-resolving model simulations, *J. Geophys. Res.*, *112*, D24S18, doi:10.1029/2007JD008728.

Twomey, S. (1977), The influence of pollution on the shortwave albedo of clouds, *J. Atmos. Sci.*, *34*, 1149–1152, doi:10.1175/1520-0469(1977)034<1149:TIOPOT>2.0.CO;2.

Wu, L., H. Su, and J. H. Jiang (2011), Regional simulations of deep convection and biomass burning over South America: 1. Model evaluations using multiple satellite data sets, *J. Geophys. Res.*, doi:10.1029/2011JD016105, in press.

Zhang, Y., R. C. Easter, S. J. Ghan, and H. Abdul-Razzak (2002), Impact of aerosol size representation on modeling aerosol-cloud interactions, *J. Geophys. Res.*, *107*(D21), 4558, doi:10.1029/2001JD001549.

Zhang, Y., R. Fu, H. Yu, R. E. Dickinson, R. N. Juarez, M. Chin, and H. Wang (2008), A regional climate model study of how biomass burning aerosol impacts land-atmosphere interactions over the Amazon, *J. Geophys. Res.*, *113*, D14S15, doi:10.1029/2007JD009449.

Zhao, C., X. Liu, L. Ruby Leung, and S. Hagos (2011), Radiative impact of mineral dust on monsoon precipitation variability over West Africa, *Atmos. Chem. Phys.*, *11*, 1879–1893, doi:10.5194/acp-11-1879-2011.

J. H. Jiang, H. Su, and L. Wu, Aura Microwave Limb Sounder (MLS) Science Team, Jet Propulsion Laboratory, California Institute of Technology, 4800 Oak Grove Dr., M/S 183-701, Pasadena, CA 91109, USA. (longtao.wu@jpl.nasa.gov)